THE ABUNDANCES OF THE HEAVIER ELEMENTS IN THE COSMIC RADIATION

W. R. Binns[a], T. L. Garrard[b], M. H. Israel[a], J. Klarmann[a], E. C. Stone[b], and C. J. Waddington[c]

a) Department of Physics and McDonnell Center for the Space Sciences, Washington University; St. Louis, Missouri 63130 USA
b) California Institute of Technology; Pasadena, California 91125 USA
c) School of Physics and Astronomy, University of Minnesota; Minneapolis, Minnesota 55455 USA

ABSTRACT

We review current work on the abundances of the ultraheavy elements in the cosmic radiation, those with $Z>30$. Those abundances are compared with predictions based on propagation and fractionation of elemental abundances from various assumed sources of the cosmic rays. We find striking similarities between the solar system and the cosmic ray source abundances for those elements with $32 \leq Z \leq 60$. For elements with $Z>60$, there appears to be a substantial enhancement in the abundances of elements synthesized in the r-process.

INTRODUCTION

At this meeting we are celebrating the 40th anniversary of the observation of "heavy" nuclei in the cosmic rays by Freier *et al.*[1,2] and Bradt and Peters[3]. Within a few years of these pioneering observations it was established that the cosmic radiation included nuclei of all the elements in the lower third of the periodic table, those up to the iron-nickel region. It was also clear that in general these elements had abundances that were not too different from those in other samples of matter found in sites of astrophysical significance, such as those in stellar atmospheres or in primitive meteoritic material. The obvious exceptions, such as the high abundances in the cosmic radiation of the generally rare elements such as Li, Be, and B, were secondary fragments produced by the interaction of heavier nuclei with the interstellar medium during the propagation of the cosmic ray nuclei to Earth.

Since these early measurements extensive studies have determined the relative abundances of all the elements lighter than nickel and of some of the more abundant isotopes with an accuracy comparable to those of the abundance determinations of other samples of matter. The abundances of these lighter nuclides in the cosmic rays are discussed in this meeting in the articles by Lund[4] and by Mewaldt[5]. However, until recently, relatively little has been known about the abundances of the nuclides beyond nickel in the periodic table, the ultraheavy or UH-nuclei, defined as those with atomic number $Z>30$. Indeed, their very presence in the cosmic radiation was not confirmed until nearly twenty years after the discovery of the heavy nuclei because they are extremely rare in cosmic rays just as they are in other samples of matter. The abrupt decrease in abundances above the iron-nickel region, where the nuclear binding energy per nucleon reaches its maximum, represents the transition from exothermic to endothermic nucleosynthesis processes where the nuclear binding energy per nucleon reaches its maximum. Figure 1 shows the meteoritic abundances compiled by Anders and

Ebihara[6] which are generally regarded as representative of the solar system and which we shall treat as a standard for purposes of comparison. The new compilation of abundances presented at this meeting by Anders and Grevesse[7] does not show major differences. The decrease beyond $_{26}$Fe is evident.

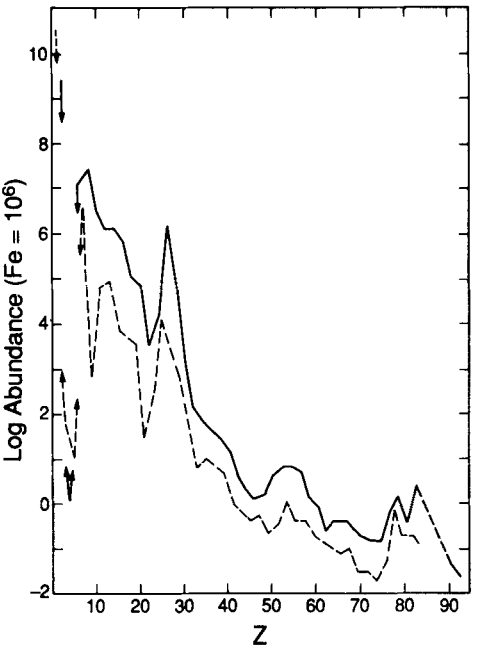

Figure 1. Elemental abundances representative of the solar system[6] plotted as a function of atomic number. The heavy solid line connects elements with even Z; the dashed line connects odd-Z elements.

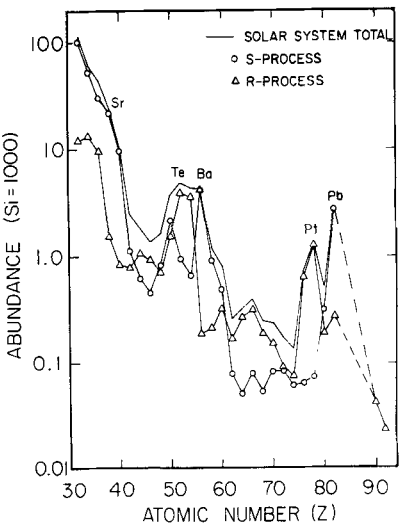

Figure 2. Decomposition of solar system abundances of even-Z elements[6] (upper line) into s-process (circles) and r-process (triangles) components.

SIGNIFICANCE OF ULTRAHEAVY COSMIC RADIATION

Studies of the UH nuclides examine material synthesized by quite different processes than those responsible for the lighter nuclides. Hence a study of the abundances of these heavier nuclides in the cosmic radiation provides a unique view of the nature of the radiation and the sources. Since the nucleosynthesis of these heavier nuclides is almost entirely due to endothermic processes of neutron capture, the abundance yields reflect the end products of synthesis occurring during the later stages of stellar evolution, when sources of neutrons and energy become available. The abundances of the lighter nuclei, on the other hand, reflect the normal nucleosynthesis processes that occur during the regular stellar evolution of main sequence stars, before they reach the late explosive stages.

The detailed features of the cosmic abundances of the trans-nickel nuclides can be satisfactorily explained as being predominantly the consequence of just two processes of nucleosynthesis; the rapid (r-) and slow (s-) processes of neutron capture. In the s-process there is sufficient time between successive neutron captures to allow β-decay to occur, while in the r-process captures occur so

frequently that nuclei are forced far beyond the limit of stability. The physics of the s-process is rather well understood, depending as it does on the β-decay and neutron capture cross-sections of observable nuclides, and the abundance distribution resulting from a given set of boundary conditions can be calculated. However, the same is not true for the r-process, which involves the properties of extremely neutron-rich, short-lived nuclides for which neither the β-decay lifetimes nor the neutron capture cross sections can be measured. As a consequence the contribution of the r-process to the solar system abundance distribution is usually deduced by subtraction of the calculated s-process contribution, with the residue being assumed to be due to the r-process.

Figure 2 shows that each process produces characteristic key elements[8]. It also illustrates the necessity of invoking some form of r-process, if only to explain the existence of the actinides, even though no convincing astrophysical site for such a process has been identified.

In addition to the information about source abundances of heavy nuclides, these studies also lead to a better understanding of the propagation of the cosmic ray nuclei through the interstellar medium. These heavier nuclei with their large nuclear cross sections are more significantly affected by nuclear absorption, and consequently less affected by other losses, such as leakage from a confinement volume, than are the lighter nuclei. Hence studies of the abundances of the UH-nuclei can give us a better definition of the parameters of the propagation models.

SHORT HISTORICAL OVERVIEW

COSMIC RAY TRACKS IN METEORITES The initial demonstration of the presence of UH-nuclei in the cosmic radiation came from the examination by Walker *et al.*[9] and Fleischer *et al.*[10,11] of tracks in meteorites due to radiation damage from heavily ionizing particles. They found many tracks which could be attributed to cosmic ray Fe nuclei near the end of their range, where they are most heavily ionizing; they also found a few tracks which were significantly longer, attributed to higher-charge nuclei with ionization rates above the threshold for damage over a longer distance. Unfortunately, the analysis of these tracks has not resulted in a charge resolution adequate to do much more than demonstrate the existence of the broadest general groups of UH-nuclei. In spite of the extremely large area-time factors available from the study of these materials and a great deal of effort by many workers, this technique has not led to reliable quantitative results.

BALLOON-BORNE INSTRUMENTS The initial observations of contemporary UH-nuclei by Fowler *et al.*[12,13] used large areas of nuclear emulsion exposed on high altitude balloons. These observations created great excitement due to an apparent large fraction of trans-bismuth events and to the report of a track corresponding to a nucleus with an apparent charge of $Z=105\pm3$. Such a superheavy nucleus would be an indicator of the hypothetical trans-actinide island of stability around $Z\sim114$. During the following decade a major international effort was made by several groups to study the UH-nuclei, resulting in a series of at least 22 separate balloon exposures of large areas of nuclear emulsions and etchable plastics. The total collecting power from this overall effort was approximately 7.6 m^2sr years, not too dissimilar from the exposures obtained by later satellite detectors.

The results obtained from these early flights, which were typically thin detectors flown at high geomagnetic cutoffs, are summarized in Figure 3, which shows the elemental abundances normalized to 10^6 iron nuclei. For comparison Figure 3 also shows solar system[6] abundances grouped for easy comparison. It can be seen that the overall agreement is fair, although the balloon data all show much higher actinide fluxes and show evidence for scanning inefficiencies at the low end of the charge scale.

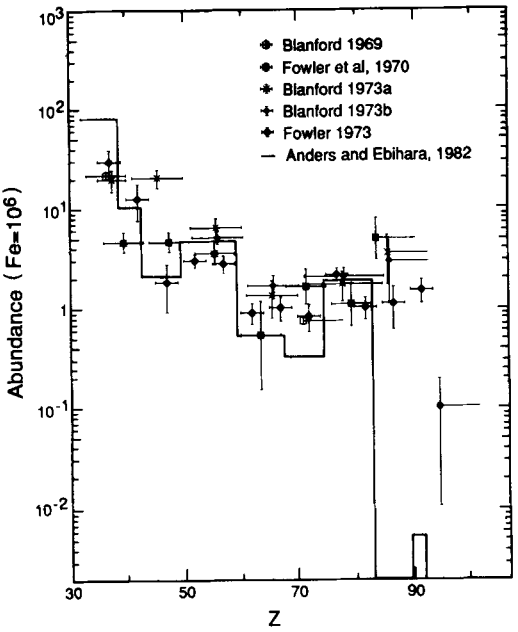

Figure 3. Results from the early balloon flights[14-18]. Cosmic ray abundances are plotted versus Z. The heavy line indicates the solar system abundances[6] summed over wide charge groups.

These detectors were designed with the assumption that the geomagnetic cutoff guaranteed that the particles were relativistic. However, Blanford *et al.*[19] showed the presence of low energy nuclei, presumably due to re-entrant albedo. Thus it was necessary to increase the thickness of the detectors in order to measure energy by observing changes in energy loss. With these thicker detectors, flights could be made at lower geomagnetic cutoffs with correspondingly increased fluxes. Improvements in the plastic detectors that occurred during this time also permitted much smaller changes in dE/dx to be measured. In addition, at this time there was a concentration of scientific interest in the highest charge nuclei, those with $Z>65$, for which contamination by even the slowest iron nuclei was not a factor.

This approach reached its culmination in a series of nine balloon flights from Sioux Falls, S.D., by the Bristol-Dublin[20] collaboration, which resulted in the detection of 97 nuclei with $Z>65$. In this study the principal detecting medium used was Lexan plastic, which is a relatively insensitive detector having measurable etch pits only for nuclei with charge-to-velocity ratios $Z/\beta>65$. In these stacks of Lexan many etch pits can be measured as the particles traverse the individual sheets, providing a series of nominally independent estimates of Z/β.

SKYLAB MEASUREMENTS The first significant space exposure of a large area passive detector was that in the Skylab[21,22]. A detector area of 1.3 m^2 was exposed for 253 days in the Skylab, which was in a 430 km altitude orbit with an inclination of 53°. The stacks of Lexan plastic, with a thickness of only about 1 g/cm^2, were mounted just inside the aluminum outer wall, also about 1 g/cm^2 thick. Particles could enter from either side, with those coming from the inside

passing through a variable amount of matter in addition to that in the opposite wall. In all 104 nuclei with $Z>65$ were observed, with a wide range of β's due to the low minimum thresholds in such a high inclination orbit. The charge spectrum deduced from these data and that reported from the Bristol-Dublin[20] balloon series both showed rather similar features, with a small peak in the platinum region, a tailing off of intensity into the actinide gap ($84 \leq Z \leq 89$) and a significant number of apparent actinide nuclei. Neither observation detected any nuclei with charges much greater than those of the actinides. In both analyses the apparent presence of an actinide gap was taken as evidence that the nuclei identified as actinides were indeed of such a high charge. Figure 4 shows charge histograms from Skylab and the Bristol-Dublin work.

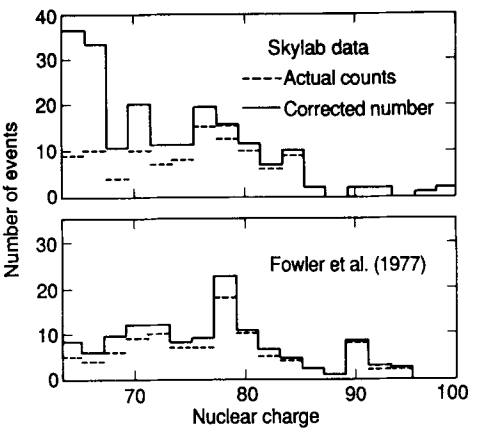

Figure 4. Charge spectra for Skylab detector and balloon data[20].

ACTIVE DETECTORS As early as 1965 Waddington[23] remarked in a rapporteur paper on reports of observations in electronic counter arrays of signals that could be attributed to the detection of nuclei with charges significantly greater than Fe. The rarity of these signals, and the sensitivity of electronic detectors to occasional random pulses, prevented any confident identification of these events as UH-nuclei. Apparently the first reported example of a contemporary UH-nucleus was the observation by Ginzberg *et al.*[24] of a single event observed in a Cherenkov counter exposed in space, which had an apparent charge of $Z>40$, from which they obtained a ratio of nuclei with $20 \leq Z \leq 28$ to those with $Z>40$ of 10^3: 1. Later Webber *et al.*[25] reported two events with $Z>40$ which they analyzed in detail in 1967[26] to obtain a value for the same ratio of 2×10^3: 1.

Techniques for building large area counters (1 to 6 m^2sr) were developed at Bristol[27] and at Washington University[28,29], but, due to limited exposure, useful results were obtained only for the more abundant elements with $Z \leq 30$[30,31]. The primary purpose of these early active detectors was to serve as prototypes of the satellite instruments flown later and their major contribution was the demonstration of the detection techniques.

SUMMARY OF EARLY EXPERIMENTS The observations of high actinide abundances were difficult to explain in terms of conventional theories of nucleosynthesis. Blake *et al.*[32] had to invoke extreme theories of nuclear stability in order to calculate β-decay rates that could describe an r-process capable of producing such high values of the abundance ratio of actinides to the lighter elements in the lead - platinum region.

There were also experimental doubts. Although the statistical weights for any one analysis are necessarily limited, it appears that significant differences exist between results reported by some of the groups, reflecting systematic uncertainties and suggesting that they can not be combined just to improve the statistics. As

early as 1979 Meyer[33] pointed out that the balloon data were not internally self-consistent, showing large changes in the charge scale from flight to flight, with the majority of the actinide events being observed in just one out of the seven flights involved.

Similarly, in the Skylab data the majority of the reported actinides were observed at very low energies, E<300 MeV/nucleon, an energy regime where charge assignments were particularly difficult, suggesting either an error in the analysis or a strikingly different energy spectrum for these actinide nuclei. Meyer[33] concluded from his analysis that the true actinide abundance was quite consistent with that expected from a source having a composition like that of the solar system, a conclusion that the later satellite results have generally confirmed. We can now understand the origin of these discrepancies since, with the availability of beams of relativistic heavy ions accelerated in the LBL Bevalac, it has become possible to both calibrate and normalize the detector materials used in these observations. Thus O'Sullivan and Thompson[34,35] showed that Lexan has a significant temperature sensitivity which increases with increasing ionization. O'Sullivan[36] has calculated that of the eleven actinide nuclei originally reported, the Z of as many as seven could have been overestimated due to the temperature effect.

PROPAGATION

A comparison of cosmic ray abundances to solar system abundances shows a significant overabundance of the rarest nuclei, as expected from the production of secondaries by nuclear interactions of cosmic rays in the interstellar medium[37,38]. Other differences likely arise from a fractionation[39,40] of the cosmic ray source material before acceleration by a process which is strongly correlated with first ionization potential (FIP). We must consider these effects to make such a comparison meaningful.

We will investigate effects of three models for the cosmic ray abundances in which the source composition is either (i) similar to the solar system, (ii) similar to the s-process (as deduced for the solar system), or (iii) similar to the r-process (again, as deduced for the solar system). We will consider two models for the FIP fractionation: (i) no fractionation, and (ii) fractionation by a multiplicative factor, f, which is a sloping step function[41] of first ionization potential (step FIP),

$$f = \begin{cases} 1 & (\mathrm{FIP} < 7 \text{ eV}) \\ \exp[-0.27\ (\mathrm{FIP}-7)] & (7 \leq \mathrm{FIP} \leq 13.6 \text{ eV}) \\ 0.168 & (\mathrm{FIP} > 13.6 \text{ eV}). \end{cases}$$

This function is based on an analysis of abundances of elements with Z≤26. Previous works[42,43,44] have shown poorer fits with fractionation described by an exponential function of FIP.

We model expected abundances in the following manner. Each set of source abundances is propagated through the interstellar medium in a standard leaky box model with a rigidity dependent path length distribution[45] using the Brewster *et al.* propagation techniques[37,38,46]. The propagation currently uses the semiempirical fragmentation cross sections of Silberberg and Tsao[47,48,49] (see also Silberberg *et al.*[50], and Waddington *et al.*[51,52]) which are calculated at 2.3 GeV/nucleon and assumed to be independent of energy.

CURRENT RESULTS: HEAO-3 HNE AND ARIEL-VI

Two different active detectors of UH-nuclei were launched into earth orbit in 1979. The results obtained from these two detectors have significantly modified the earlier results described above and are largely responsible for our present state of knowledge about these nuclei in the cosmic radiation. These two detectors, Ariel-VI[53] and the High Energy Astronomical Observatory Heavy Nuclei Experiment[54], the HEAO-3 HNE, both consisted of electronic detectors with sufficient collecting power, dynamic range, and charge resolution to study the entire charge spectrum from <26 to >100. Both combined a measurement of the rate of energy loss (dE/dx) in a gas with a measurement of the Cherenkov light emission from a plastic radiator. The HEAO instrument determined dE/dx using parallel-plate pulse ionization chambers, while Ariel measured the light emitted by the scintillation in the gas.

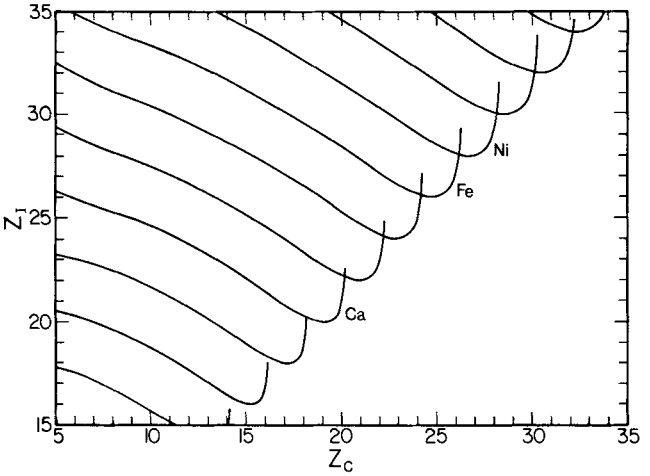

Figure 5. Schematic illustration of $Z_I = \sqrt{dE/dx}$ versus $Z_C = \sqrt{C}$ for HEAO or Ariel. Each line is the locus of average signals from nuclei of various energies and specified charge. In HEAO energy specifies the position along a line.

The basic concept of particle identification by a combination of signals that measure dE/dx and Cherenkov output is illustrated in Figure 5. To first order, both dE/dx and the Cherenkov signal, C, are proportional to Z^2, but they have quite different β-dependences. As a result the combination of the two signals produces an unambiguous measure of Z and β, except at the highest energies where the relativistic rise in ionization produces a hook in the dE/dx vs C curve. If the particles are known to be of high energy, as, for example, when the spacecraft is in a part of the orbit where the geomagnetic cut-off rigidity is high, then the Cherenkov signal is independent of velocity and can be used as a measure of Z. Thus the HEAO group obtained a good resolution subset of their data by selecting only those events where the geomagnetic cutoff rigidity was greater than 8 GV and considering only the Cherenkov signal.

Ariel-VI was launched on 3 June 1979 into a near circular orbit with a 625 km altitude and an inclination of 55°. Figure 6 is a schematic cross section of the Ariel-VI instrument[53,55]. The instrument makes use of a clever design concept to produce a relatively simple device with a large effective collecting power. The detector is a gas-filled sphere, with the gas scintillating in proportion to dE/dx. Inside the sphere is a shell of plastic Cherenkov radiator. The scintillation and

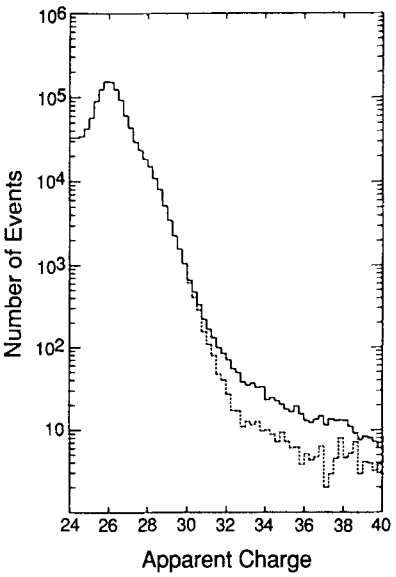

Figure 7. Ariel[55] charge histogram in the Fe region. The solid line is the total spectrum including stopping Fe, and the dashed line is the clean spectrum, collected at cutoffs above 3.4GV.

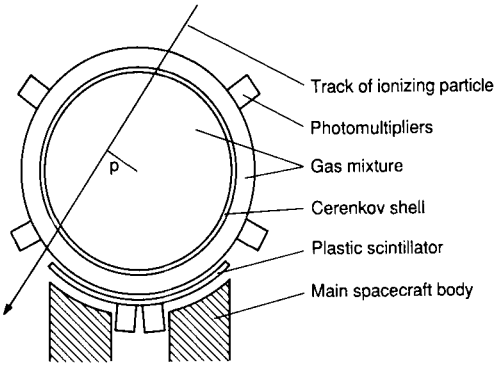

Figure 6. Schematic of the Ariel instrument.

Cherenkov light are collected by the same photomultipliers, with the slow scintillation pulse being distinguished from the fast Cherenkov pulse by electronic pulse shape discriminators. Both the magnitude of the scintillation signal, S, and the Cherenkov signal, C, depend on the trajectory of the particles through the instrument; C increases and S decreases with impact parameter, p. With no hodoscope to measure the trajectory one might expect serious smearing of the charge resolution. However, the relative dimensions of the scintillator sphere and the Cherenkov shell were carefully selected so that the locus of points in the C, S plane corresponding to particles of a given Z and β but varying p, is almost coincident (neglecting those few particles on the relativistic rise hook) with the locus for a given Z and p but varying β. Hence the instrument cannot uniquely determine either p or β, but the combination of C and S is sufficient to provide a measure of Z.

The HEAO-3 HNE instrument was launched on 20 September 1979 into a near circular orbit with a 495 km altitude and an inclination of 43.6°. Figure 8 is a schematic cross section of the HNE instrument[54]. It had two sets of three dual-gap ionization chambers, one on each side of the Cherenkov counter. The Cherenkov counter consisted of two pieces of Pilot 425 radiator viewed by eight photomultipliers. On each side of each set of ion chambers, and sharing their pressure vessel, was an x - y pair of hodoscope layers for trajectory information. The hodoscopes permitted correction of the measured signals for the path length in each detector and for the non-uniformity of response over the area.

Both of these instruments were able to study the abundance peak at Fe to demonstrate their charge resolution. Figures 7 and 9 show published charge spectra in the Fe region that are comparable. Selections were applied to the data in order to improve the resolution of the sample under examination at the cost of statistical weight. The effect of varying the selection criteria on the HEAO-3 data is shown in Figure 10, which illustrates the loss in resolution as the selection criteria are relaxed.

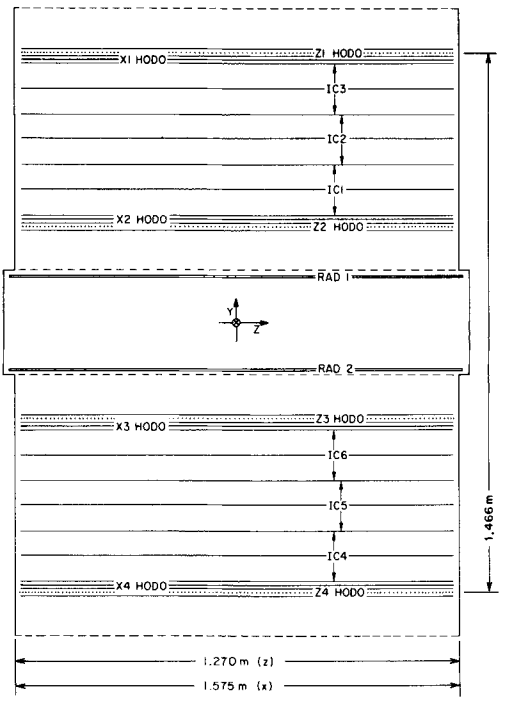

Figure 8. Schematic of the HEAO HNE instrument. Abbreviations label the HODOscopes, RADiators, and Ion Chambers. The dashed lines indicate locations of the "thin" windows in the pressure vessels.

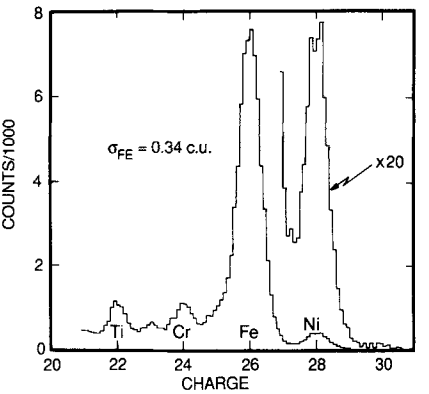

Figure 9. HEAO charge histogram[42] of nuclei in the Fe region which have either low energy or high rigidity. The line labeled × 20 has been scaled up to show the shape of the nickel peak.

Fewer selections were possible on the Ariel data due to the much smaller number of parameters that were measured for each particle. Thus the published results from Ariel cover wider charge ranges than the early reports of HEAO data[8,42,56,57], which tended to be specific for each part of the charge spectrum. In comparing data from the two instruments it should be remembered that the mean energy of the particles observed by Ariel is appreciably lower than that of the particles observed by HEAO due to the greater inclination of the Ariel orbit.

HEAO HIGHEST RESOLUTION CHARGE SPECTRUM: $32 \leq Z \leq 42$ The pre-satellite abundance measurements summarized above had generated a great deal of interest in r- and s-process abundances in the cosmic rays. While the elements that lie just above the iron-nickel peak may have a complicated history of nucleosynthesis, with possible contributions from explosive nucleosynthesis processes such as C detonation and helium flashes, for elements with $Z > 34$ the r- and s-processes dominate the production. For the relatively abundant elements in the $32 \leq Z \leq 42$ charge region, the HEAO data could be strongly selected to maximize charge resolution. Thus Binns *et al.*[42,43] combined data from two groups of nuclei, those with low energy and those with high rigidity. The resolution obtained by HEAO with such a selection is illustrated in Figure 9 for elements in the iron-nickel region, and can be characterized by a charge resolution (standard deviation, σ) of 0.34 charge units. The same selections applied to those nuclei with $Z > 32$ give the

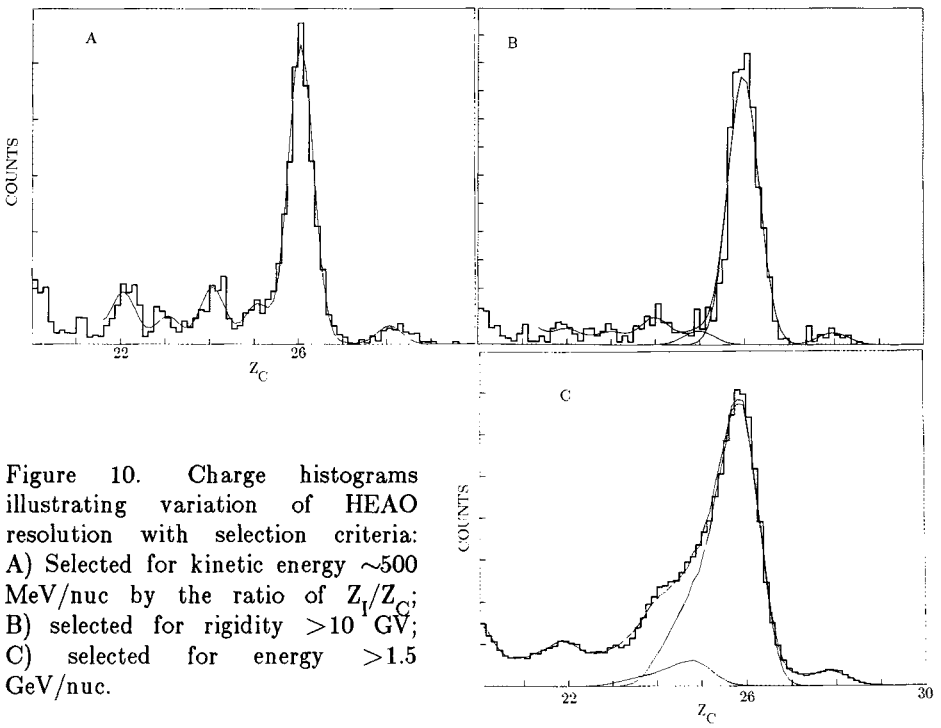

Figure 10. Charge histograms illustrating variation of HEAO resolution with selection criteria: A) Selected for kinetic energy ~500 MeV/nuc by the ratio of Z_I/Z_C; B) selected for rigidity >10 GV; C) selected for energy >1.5 GeV/nuc.

distribution shown in Figure 11, where this data set corresponds to the observation of 2.6 x 10^6 iron nuclei. Clear peaks are seen at the even charge elements from $_{32}$Ge to $_{38}$Sr and convincing upper limits can be placed on the abundances of odd Z elements. These data were fit with a gaussian maximum likelihood algorithm to derive the elemental abundances and showed a distribution with σ = 0.40 c.u. at Z=32 increasing linearly by 0.016 c.u. per charge as Z increased. The best fit is shown as the smooth curve.

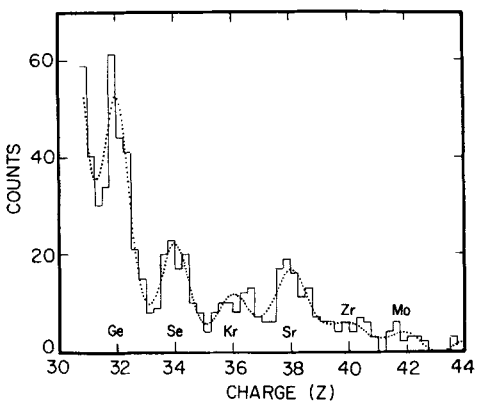

Figure 11. Charge histogram for 32≤Z≤42, selected for high resolution in the same way as the Fe events shown in Figure 9.

These abundances are compared to those derived by propagating various source models in Figure 12. In the comparison to propagated solar system abundances (Cameron[58] for historical reasons) the agreement is good and is clearly improved by making a correction for fractionation based on FIP. The comparison

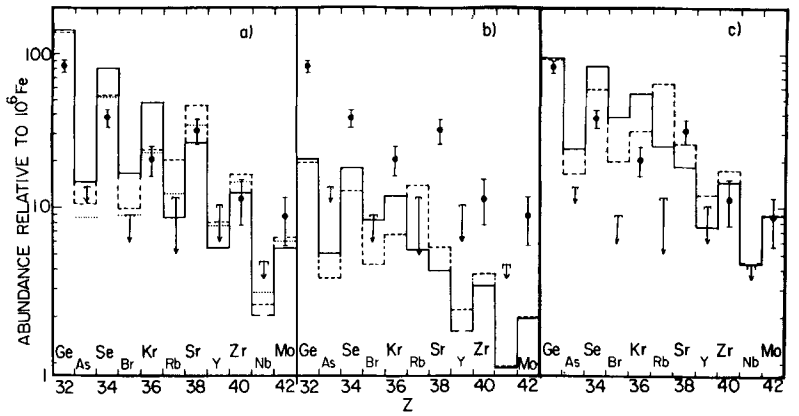

Figure 12. Comparison of HEAO abundances with various source models and various fractionation models, after propagation. Panel a: solar system abundances[58] without fractionation (solid line), with exponential FIP (dashed line), and with step FIP (dotted line). b: r-process[58] without fractionation (solid) and with exponential FIP (dashed). c: like b, but renormalized.

to propagated r-process is obviously not useful, even if we take the normalization to Fe as a free parameter (panel c). The cosmic rays have much larger abundances for $_{38}$Sr than for $_{37}$Rb, as is seen in the solar system and in contradiction to predictions based on r-process.

HEAO CHARGE SPECTRUM: $50 \leq Z \leq 58$ The elements in the region from $_{50}$Sn to $_{58}$Ce have abundances that are strongly dependent on the relative proportion of r- and s- process nucleosynthesis that has occurred and can provide characteristic signatures for each process. However, the abundances in this charge region are significantly less than those in the light UH-nuclei region and as a consequence the HEAO data could not be as tightly selected. Hence the charge resolution was not as good as for the lighter nuclei and it was more difficult to determine the abundances of the individual elements. In an initial analysis of the data[56] events were selected by requiring that they either occurred at high geomagnetic cutoff (contributing 60% of the events) or were clearly of high energy from the Cherenkov and ion chamber signals (40%). The resulting charge spectrum (Figure 13) has poorer charge resolution because of these looser selections. However, it was still possible to observe individual charge peaks for the even charge elements and to determine abundances relative to one of the elements in this group.

Again, the cosmic ray abundances, shown in Figure 14, are generally inconsistent with pure r-process source material. The measurements can be fit by either solar system type source material, with FIP fractionation (as observed at lower Z) or with s-process source material without fractionation.

COMBINED DATA SET Abundances over the entire charge range, $33 \leq Z \leq 86$, have been derived in recent HEAO work[44,59,60], applying uniform selection criteria to produce a data set similar to those described in Ariel publications. Charge histograms for this recently selected HEAO data set are shown in Figure 15 with the corresponding Ariel-VI abundance measurements[55]. The charge resolution can be seen to be adequate to resolve even-odd element pairs up to Z=60. The

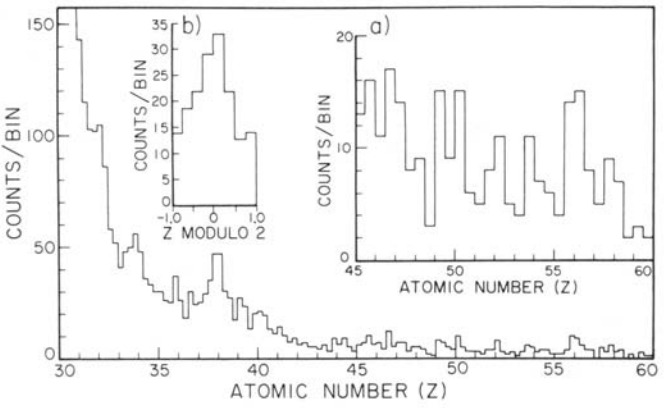

Figure 13. Charge histogram for a data set[56] selected for acceptable statistics in the $50 \leq Z \leq 60$ charge region. The insets show (a) an expanded view of the peaks in that charge region and (b) a modulo 2 histogram of that region.

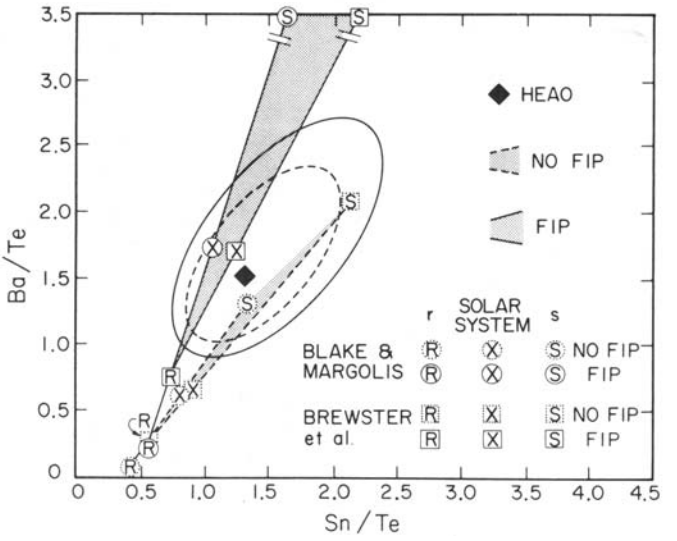

Figure 14. HEAO[56,61] measured abundance ratios plotted with propagated r-, s-, and solar sys.[58] abundances with and without FIP fractionation. The two error contours indicate 50% and 68% probabilities of containing the actual value. The two propagations[62,37,38] give an indication of the uncertainty due to variations in techniques of propagation.

abundances, derived from the fits illustrated in Figure 15, are tabulated in Table 1. The HEAO and Ariel results are compared in Figure 16, showing excellent agreement between the two measurements. Since the various HEAO and Ariel data sets are so similar, it is useful to combine the data, reducing the statistical uncertainties. In combining the data, we have used the weighted average of our abundances reported here with those of Ariel-VI for most elements. For $Z = 32$ and for the $Z = 41,42$ pair, we feel that the earlier HEAO measurement[42,43] (with better resolution than either this HEAO data set or Ariel-VI) should be used. For the "actinides" ($88 \leq Z \leq 100$) we have scaled our previously reported actinide/Pt-Pb ratio[57] with the currently reported Pt-Pb/Fe ratio to derive an actinide/Fe ratio. That ratio is averaged with that of Ariel-VI. The current Ariel-VI value for the actinide/Pt-Pb ratio is somewhat larger than ours but statistically similar. The resultant data set, covering the Z range from 32 to 100, is our best estimate for abundances of ultraheavy galactic cosmic rays (UHGCRs) and is shown in Table 1.

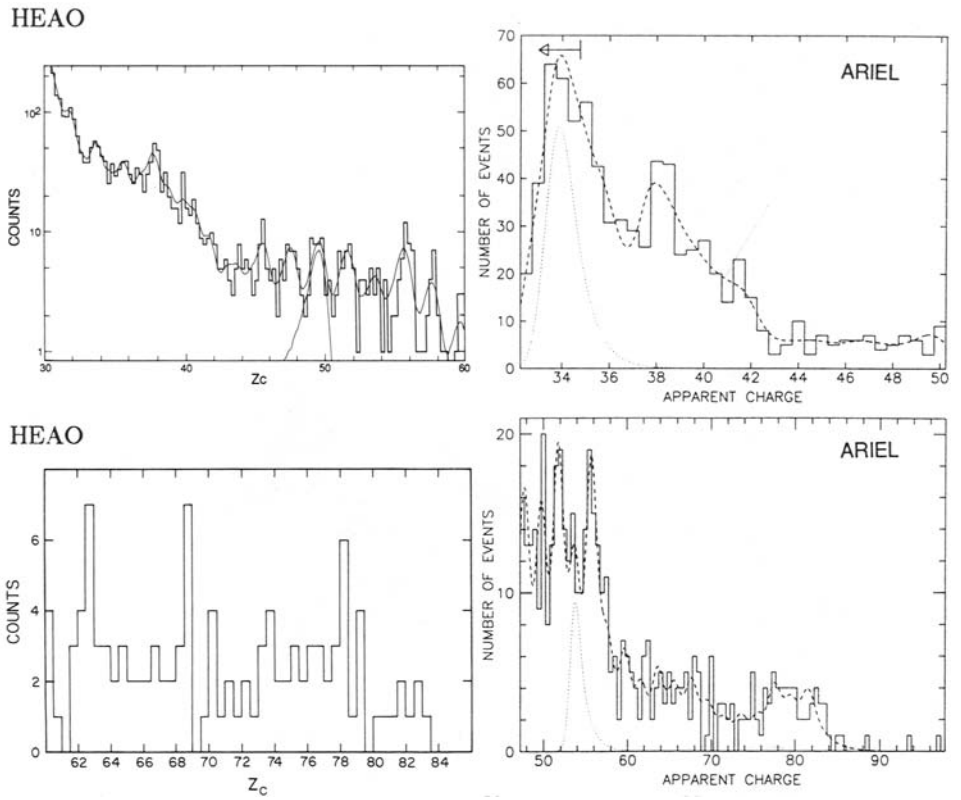

Figure 15. Charge histograms for HEAO[59] (left) and Ariel[55] (right) for various Z ranges. The light (HEAO) and dashed (Ariel) lines indicate fits from which abundances are derived.

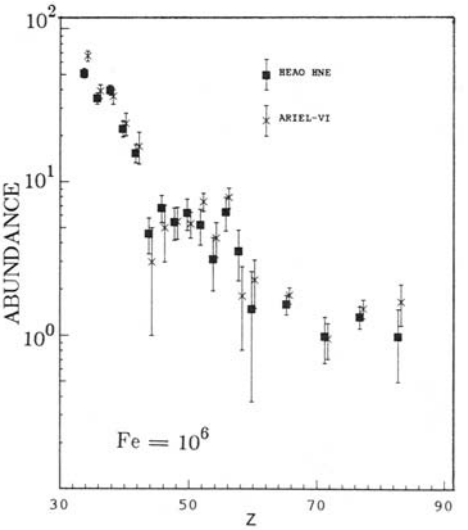

Figure 16. Comparison of Ariel[55] and HEAO abundances[59] relative to Fe over an extended charge range, $33 \leq Z \leq 86$. The abundances above Z=60 are normalized to the widths of the charge bins. Un-normalized abundances are in Table 1.

Relative Abundances (Fe=10^6)					
element	HEAO	sys	Ariel	previous	UHGCR
32	- -	-	- -	91 $^{+12}_{-8}$	91 $^{+12}_{-8}$
33-34	51.2±3.7	6.0	66 ±5	52 ± 6	61.1 ± 4.1
35-36	35.1±3.0	1.0	39 ±4	30 ± 8	36.6 ± 2.5
37-38	39.6±3.1	2.7	36 ±4	43 ± 6	37.8 ± 2.9
39-40	22.2±2.6	1.2	24 ±4	18 ± 5	22.8 ± 2.3
41-42	[15.4±2.1]	2.5	17 ±4	11 ± 3	11.0 ± 3.0
43-44	4.6±1.2	0.3	3 ±2	- -	4.1 ± 1.1
45-46	6.7±1.4	0.4	5 ±2	- -	6.2 ± 1.1
47-48	5.5±1.3	0.3	5.5±1.3	- -	5.5 ± 0.9
49-50	6.3±1.5	0.2	5.3±1.0	5.7 ± 1.3	5.6 ± 0.8
51-52	5.2±1.4	0.3	7.4±1.0	3.0 ± 1.0	6.7 ± 0.8
53-54	3.1±1.2	0.6	4.3±1.1	3.5 ± 0.9	3.8 ± 0.8
55-56	6.3±1.6	0.5	7.9±1.2	6.2 ± 1.0	7.4 ± 1.0
57-58	3.5±1.3	0.4	1.8±1.0	2.8 ± 0.9	2.4 ± 0.8
59-60	1.5±1.1	0.1	2.3±0.8	- -	2.0 ± 0.7
LS(62-69)	6.4±0.9	-	7.3±0.9	3.54± 0.63	6.9 ± 0.6
HS(70-73)	$2.0^{+0.7}_{-0.5}$	-	1.9±0.5	$1.04^{+0.45}_{-0.33}$	1.9 ± 0.4
Pt(74-80)	5.1±0.8	-	5.7±0.8	4.38± 0.71	5.4 ± 0.6
Pb(81-83)	$1.2^{+0.6}_{-0.4}$	-	2.0±0.6	$1.04^{+0.45}_{-0.33}$	1.6 ± 0.4
Actinide (88-100)	- -	-	0.4±0.2	$0.06^{+0.14}_{-0.05}$	$0.13^{+0.12}_{-0.05}$

Table 1. Comparison of measured abundances for HEAO-3 HNE[59] and Ariel-VI[55]. The data labeled previous are from HEAO[8,43,57,61]. An estimate of the systematic uncertainty due to the deconvolution procedure for HEAO[59] is in the column labeled "sys". The previous HEAO work tabulated here is based on data sets with resolution good enough that such uncertainties are small. However, there are uncertainties in the normalization to Fe in the older works. The column labeled UHGCR is a combined result as described in the text.

In Figure 17a we show the ratio of the UHGCR abundances to the calculated abundances for a solar system source, without FIP fractionation. As we expect from the preceding discussion, the trend of the data is generally the same as the calculation, but there are deviations of roughly a factor of two. It should be noted that the error bars indicated in Figure 17a (and the succeeding figures) are uncertainties of the UHGCRs only. There are significant additional uncertainties associated with the cross sections, with the source abundances, and with the possibility of variations of the energy spectra with charge like that observed for secondaries[63]. We calculate a goodness of fit parameter, χ^2, between the UHGCR abundances and the model abundances. However, since only the statistical measurement uncertainties in the UHGCR abundances are included the reduced χ^2

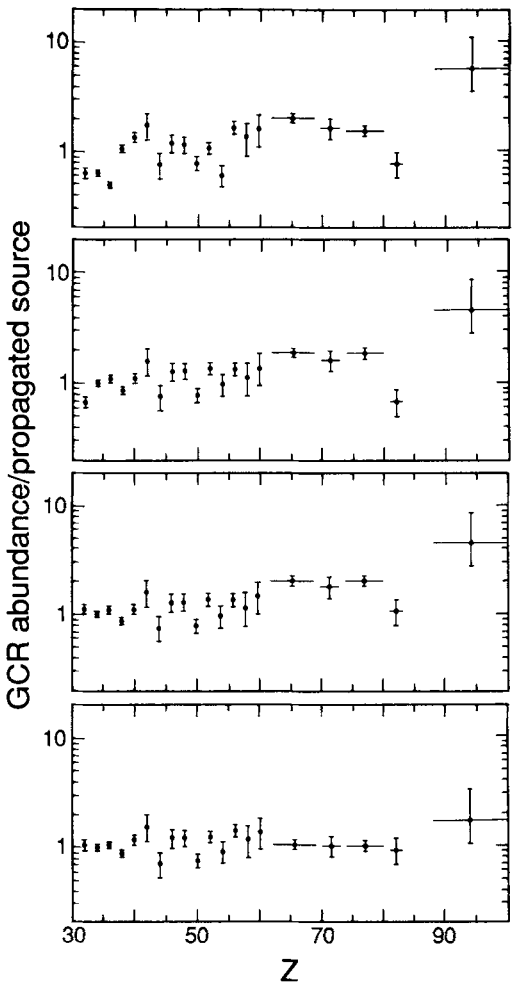

Figure 17. Ratios of UH galactic cosmic ray abundances to abundances calculated with various models for cosmic ray source material and fractionation. a) solar system[6] source with no fractionation; b) solar system source with step FIP fractionation; c) solar system[6] source with corrected[64] Pb, Ge and with step FIP; d) "best source" as described in the text, with step FIP.

values are typically much larger than 1. These χ^2 values still provide useful discrimination between various source models and are given in Table 2 for all the models discussed here.

If we include the step FIP fractionation in the calculation, then the agreement between the calculation and the measurements is much better, confirming the observation from abundances of elements with lower Z that FIP organizes the ratios of abundances of galactic cosmic rays to solar system abundances. This agreement is illustrated by Figure 17b and by the improved value of χ^2. The UHGCR abundances agree with the solar system source with step FIP to within $\pm 35\%$ from charge 32 to 60, with the most significant difference occurring at $_{32}$Ge. If we allow the normalization to iron to vary as a free parameter (K) then the best fit value of K is 0.1% larger than that of the solar system, a negligible distinction. Over the restricted charge range, $32 \leq Z \leq 60$, the best fit K is 4% smaller than the solar system, still negligible. Above $Z = 60$, we find that "Pb" is substantially low and that "Pt", "HS", "LS", and "actinides" are substantially high.

One possible explanation[8] for the relatively low abundance of $_{82}$Pb and $_{32}$Ge would be a volatility related fractionation process instead of FIP fractionation. Apart from these two elements, FIP and volatility are closely correlated and we cannot distinguish between these fractionation models. Alternatively, Grevesse and Meyer[64] have re-examined spectroscopic data on photospheric abundances and have suggested that the photospheric abundance of Pb is about 0.63 of the standard[6] meteoritic abundance and the photospheric abundance of Ge is about 0.61 of the standard meteoritic abundance. Thus, the UHGCR Pb and Ge abundances would be in agreement with that of the solar photosphere, but different from the meteoritic abundances. This distinction is also reported in Anders and Grevesse[7], this conference. In figure 17c we show a comparison of UHGCR abundances with an accordingly modified solar system, with FIP fractionation. As expected, the fit is much improved for the two modified elements, Pb and Ge (See Table 2.). Margolis and Blake[69] have suggested that low Pb abundances could result from limited recycling in the s-process due to insufficiently intense neutron exposures.

K	α	G&M	FIP	Z range	χ^2_ν	ν	comment
1	1	no	no	32-100	20.6	20	Comparison to propagated solar system[1], Figure 17a.
1	1	no	step	32-100	4.87	20	as above, but with FIP fractionation, see 17b.
1.001	1	no	step	32-100	5.13	19	as above, but allowing the Fe normalization to vary.
0.96	1	no	step	32-60	3.12	14	as above, but with restricted Z range.
1.07	1	yes	step	32-100	3.80	19	using the G&M correction, see Figure 17c.
1.02	1	yes	step	32-60	1.94	14	see again Figure 17c.
1.05	0.86	yes	step	35-60	2.32	11	with best fit value of α.
1.45	0.18	yes	step	62-100	0.15	3	
1.45	0.40	yes	no	62-100	1.95	3	
best source			step	32-100	1.31	20	see Figure 17d.

Table 2. Parameters of fits to the propagated abundances for models of the cosmic ray source material given by $K\times(\alpha\times s + (2\text{-}\alpha)\times r)$ where r and s represent the r- and s-process components of the solar system abundances. K determines the Fe normalization; K=1 is the solar system value. The parameter α determines the s/r mix; $\alpha = 1$ is the solar system mix. K or α values in the table of 1 reflect constrained values, not free parameters. Reduced χ^2 is specified; degrees of freedom are given by ν. The column header G&M indicates the correction[64] to Pb and Ge.

However, none of these explanations for the relatively low Pb abundance affects the observation that Pt and its secondaries are overabundant relative to Fe. The secondary abundances are likely high just because the abundance of the Pt group primaries which produce them are high. The Pt group is known to be an indicator of r-process nucleosynthesis, so we have calculated model abundances for an r-process source. The r-process source abundances are taken from Binns *et al.*[8] and modified by subtracting the Grevesse and Meyer[64] correction from the Pb. Fractionation and propagation were modeled as described earlier, i.e., sloping step

function FIP fractionation and propagation according to Brewster *et al.*[37,38,46] While the charge region below 60 shows poor agreement with an r-process source, with the observed values of s-process elements such as $_{38}$Sr, $_{40}$Zr, and $_{56}$Ba showing large overabundances, a pure r-process source does organize the Z>60 points much better than a solar system source. The UHGCRs in this charge region are roughly three times more abundant than solar system r-process. We can use a two parameter fit to determine how large an enhancement of r-process source material is present. If we interpret the Z>60 abundances relative to Fe as a mixture of r-process and s-process components fractionated by step FIP, then the best fit s/r ratio is 0.10 times that of the solar system, with an upper limit (84% confidence level) of 0.25 and a lower limit of 0. A pure r-process source without FIP fractionation does not fit as well. If we assume a fractionated r-process source, or the best fit mixture listed in Table 2, then the secondary (LS, HS) to primary (Pt) ratio for $Z \geq 60$ is consistent with the simple standard leaky box model. No more elaborate model is justified, especially in view of the paucity of the statistics and the uncertainties in the cross sections[51,52].

We can also examine the UHGCR abundances of elements with $Z \leq 60$ for r-process enhancements, but expect little enhancement since the solar system source model fits well. If we consider the abundances for $35 \leq Z \leq 60$ only (32, 33, and 34 abundances in the solar system have contributions from other nucleosynthetic processes) and interpret them as a mixture of r- and s-process components fractionated by step FIP, then the best fit s/r ratio is 0.76 ± 0.17 times that of the solar system, similar to earlier reports[56,61]. This ratio differs significantly from that given for the $Z \geq 60$ charge range.

DISCUSSION AND CONCLUSIONS

The elements in the range $32 \leq Z \leq 60$ are well fit by the model which assumes a solar system source with step FIP fractionation; over the charge range $35 \leq Z \leq 60$ they are somewhat better fit with a r/s mixture with a small r-process enhancement; Pt and its secondaries are best fit by an r-process source with either no FIP or step FIP; and the Pb and Ge abundances resemble those of the photosphere[64] rather than meteorites. We have therefore compiled a best model for the source composition with all these features: for Z=32 the source abundance is given by Grevesse and Meyer[64]; for Z=33,34 the source abundance is given by Anders and Ebihara[6]; for $35 \leq Z \leq 60$ the source abundances are given by by $1.05 \times (0.86 \times s + 1.14 \times r)$, where r and s are based on our decomposition[8] of the solar system[6]; for $62 \leq Z \leq 100$ the "best" source abundances are given by $1.45 \times (0.18 \times s + 1.82 \times r)$ where our r-process abundances have been corrected per Grevesse and Meyer[64].

In Figure 17d we show a comparison of UHGCR abundances with those given by our best source, after FIP fractionation and propagation. Table 3 shows these best source abundances both before and after FIP fractionation. The abundances before fractionation are indicative of the nucleosynthesis history of the UH nuclides; the fractionated abundances presumably result from the ionization state of the injected material or of the source of the injected material as observed in the solar corona. Estimation of uncertainties is quite difficult. Elements which have similar abundances in the UHGCR and in the best source should be predominantly primary in the cosmic radiation and hence the uncertainties in the source should be comparable to those in the UHGCRs. Source abundances less than 1 per 10^6 Fe

Z	UHGCR	best source unfrac	best source frac	comment
32	91+12,-8	80.0	79.4	G & M[64]
33	61.1±4.1	7.54	4.47	A & E[6]
34		69.0	41.6	
35	36.6±2.5	14.7	5.07	
36		57.8	12.3	
37	37.8±2.9	9.14	11.6	
38		24.7	31.2	
39	22.8±2.3	4.74	6.00	
40		11.2	14.1	
41	11±3	0.72	0.91	
42		3.00	2.34	
43	4.1±1.1	0.0	0.0	
44		2.27	2.60	
45	6.2±1.1	0.44	0.49	
46		1.70	1.49	best fit
47	5.5±0.9	0.66	0.71	r, s mix:
48		1.85	1.36	K = 1.05
49	5.6±0.8	0.23	0.29	α = 0.86
50		4.38	5.06	
51	6.7±0.8	0.44	0.36	
52		6.23	4.58	
53	3.8±0.8	1.18	0.59	
54		5.56	1.76	
55	7.4±1.0	0.48	0.61	
56		4.49	5.68	
57	2.4±0.8	0.49	0.61	
58		1.25	1.58	
59	2.0±0.7	0.20	0.26	
60		0.97	1.23	

Z	UHGCR	best source unfrac	best source frac	comment
62	6.9±0.6	0.55	0.70	best fit r,s mix: K = 1.45 α = 0.18
63		0.27	0.34	
64		0.83	1.06	
65		0.16	0.20	
66		0.95	1.21	
67		0.24	0.30	
68		0.60	0.76	
69		0.09	0.12	
70	1.9±0.4	0.49	0.62	
71		0.09	0.12	
72		0.29	0.37	
73		0.04	0.05	
74	5.4±0.6	0.24	0.23	
75		0.14	0.14	
76		1.93	1.54	
77		1.90	1.36	
78		3.82	2.82	
79		0.52	0.36	
80		0.67	0.34	
81	1.6±0.4	0.23	0.29	
82		2.36	2.66	
83		0.34	0.40	
90	0.13+0.12 -0.05	0.09	0.11	
92		0.02	0.03	

Table 3: Compilation of "best source" abundances, relative to 10^6 Fe. The UHGCR abundances are repeated from Table 1 to indicate uncertainties in source abundances; read the discussion of uncertainties in the text. Source abundances less than 1 are highly uncertain.

are highly uncertain because the corresponding cosmic ray abundances are dominated by secondary production. Further uncertainties are introduced by the inadequate statistics and resolution which require us to analyze element pairs and groups rather than individual elements.

The r-process enhancement above Z = 60 might indicate the admixture of some "unusual" r-process material in a medium which is otherwise roughly similar to the solar system in composition. This r-process admixture is unusual only in the sense that it is not the same as in the solar system; it is not difficult to model an r-process which synthesizes additional nuclei with Z>60[65]. As for the s-process, a calculated r-process abundance spectrum depends on such parameters as neutron bombardment flux and exposure time. Adjustment of these parameters allows modification of the spectrum; in particular, the regions separated by "magic" numbers of protons or neutrons can be enhanced or suppressed relative to each other. The observed r-process enhancement places some limits on physical conditions where cosmic ray nuclei are synthesized and represents evidence that these conditions differ from those where the solar system material was produced. If

the LDEF experiment[36] is recovered in 1990 and if it functions as hoped in spite of its extra exposure time, it may lead to a better understanding of these differences.

The secondaries in the $40 \leq Z \leq 49$ interval are well fit by a standard propagation model without invoking truncation of path lengths[66,67], continuous acceleration[68], or other elaborations of the standard model. If we assume an r-process source to explain the overabundance of the Pt relative to the solar system, then the abundances of the HS and LS groups can also be explained without any elaborations on the simple model.

The UHGCR abundances are, in general, measurably different from those expected from solar system abundances. They indicate nucleosynthesis of the heaviest nuclei in an environment with enhanced r-process. The r-process deduced for the source of the ultraheavy cosmic rays differs from that inferred from solar system abundances.

ACKNOWLEDGEMENTS

This research was supported in part by NASA under grants NAG 8-498, 500, and 502; and NGR 05-002-160, 24-005-050, and 26-008-001.

REFERENCES

1) Freier, P. S., E. J. Lofgren, E. P. Ney, F. Oppenheimer, H. L. Bradt and B. Peters, *Phys. Rev.* **74**, 213, 1948
2) Freier, P. S., E. J. Lofgren, E. P. Ney and F. Oppenheimer, *Phys. Rev.* **74**, 1818, 1948
3) Bradt, H. L., and B. Peters, *Phys. Rev.* **74**, 1828, 1948
4) Lund, N., *Symposium on Cosmic Abundances of Matter (Minneapolis)*, AIP Conf. Proc., 1988
5) Mewaldt, R. A., *op. cit.*, 1988
6) Anders, E. and M. Ebihara, *Geochim. et Cosmochim.* **46**, 2363, 1982
7) Anders, E. and N. Grevesse, *Symposium on Cosmic Abundances of Matter (Minneapolis)*, AIP Conf. Proc., 1988
8) Binns, W. R., N. R. Brewster, D. J. Fixsen, T. L. Garrard, M. H. Israel, J. Klarmann, B. J. Newport, E. C. Stone, and C. J. Waddington, *Astrophys. J.* **297**, 111, 1985
9) Walker, R. M., R. L. Fleischer and P. B. Price, *Proc. 9th Int. Cosmic Ray Conf. (London)* **2**, 1086, 1965
10) Fleischer, R. L., P. B. Price, R. M. Walker, and M. Maurette, *J. Geophys. Res.* **72**, 331, 1967
11) Fleischer, R. L., P. B. Price, R. M. Walker, M. Maurette, and G. Morgan, *J. Geophys. Res.* **72**, 355, 1967
12) Fowler, P. H., R. A. Adams, V. G. Cowen and J. M. Kidd, *Proc. Roy. Soc. A* **301**, 39, 1967
13) Fowler, P. H., V. M. Clapham, V. G. Cowen, J. M. Kidd and R. T. Moses, *Proc. Roy. Soc. A* **318**, 1, 1970
14) Blanford Jr., G. E., M. W. Friedlander, J. Klarmann, R. M. Walker, J. P. Wefel, W. C. Wells, R. L. Fleischer, G. E. Nichols, and P. B. Price, *Phys. Rev. Lett.* **23**, 338, 1969
15) Fowler, P. H., J. M. Kidd, and R. T. Moses, *Proc. 11th Int. Cosmic Ray Conf., Acta Physica Hung. Supp. 1* **29**, 399, 1970
16) Blanford Jr., G. E., M. W. Friedlander, J. Klarmann, S. S. Pomeroy, R. M. Walker, J. P. Wefel, P. H. Fowler, J. M. Kidd, E. J. Kobetich, R. T. Moses and R. T. Thorne, *Phys. Rev. D.* **8**, 1707, 1973
17) Blanford Jr., G. E., M. W. Friedlander, J. Klarmann, R. M. Walker, and J. P. Wefel, *Phys. Rev. D.* **8**, 1722, 1973
18) Fowler, P. H., *Proc. 13th Int. Cosmic Ray Conf. (Denver)* **5**, 3627, 1973
19) Blanford, G. E., M. W. Friedlander, J. Klarmann, S. S. Pomeroy, R. M. Walker, and J. P. Wefel, *J. Geophys. Res.* **77**, 6037, 1972
20) Fowler, P. H., D. L. Henshaw, C. O'Ceallaigh, D. O'Sullivan, and A. Thompson, *Proc. 15th Int. Cosmic Ray Conf. (Plovdiv)* **11**, 161, 1977
21) Price, P. B., and E. K. Shirk, *Proc.*

14th Int. Cosmic Ray Conf. (Munich) **1**, 268, 1975
22) Shirk, E. K. and P. B. Price, *Astrophys. J.* **220**, 719, 1978
23) Waddington, C. J., *Proc. 9th Int. Cosmic Ray Conf. (London)* **1**, 462, 1965
24) Ginzberg, V. L., L. V. Kurnosova, L. A. Razorenor and M. L. Fradkin, *Space Sci. Rev.* **2**, 778, 1963
25) Webber, W. R., J. F. Ormes, T. Von Rosenvinge, *Proc. 9th Int. Cosmic Ray Conf. (London)* **1**, 407, 1965
26) Ormes, J. F., T. von Rosenvinge, and W. R. Webber, *Astrophys. J.* **147**, 1205, 1967
27) Fowler, P. H., R. J. Edge, R. T. Moses, N. O. Tatham, C. Thoburn, R. N. F. Walker and A. Worley, *Proc. 15th Int. Cosmic Ray Conf. (Plovdiv)* **11**, 174, 1977
28) J. W. Epstein, J. I. Fernandez, M. H. Israel, J. Klarmann, and R. A. Mewaldt, *Nucl. Inst. Meth.* **95**, 77, 1971
29) Love, P. L., J. Tueller, J. W. Epstein, M. H. Israel, and J. Klarmann, *Nucl. Inst. Meth.* **140**, 569, 1977
30) Mewaldt, R. A., J. I. Fernandez, M. H. Israel, J. Klarmann, *Astrophys. Sp. Sci.* **22**, 45, 1973
31) Tueller, J., P. L. Love, M. H. Israel, and J. Klarmann, *Astrophys. J.* **228**, 582, 1979
32) Blake, J. B., K. L. Hainebach, D. N. Schramm, and J. D. Anglin, *Astrophys. J.* **221**, 694, 1978
33) Meyer, J. P. *Proc. 16th Int. Cosmic Ray Conf. (Kyoto)* **1**, 374, 1979
34) O'Sullivan, D. and A. Thompson, *Nuclear Tracks* **4**, 271, 1980
35) Thompson, A. and D. O'Sullivan, *Proc. 12th Track Conf.*, Pergamon Press, 1983
36) O'Sullivan, D., *Irish Astro. J.* **17**, 40, 1985
37) Brewster, N. R., P. S. Freier, and C. J. Waddington, *Astrophys. J.* **264**, 324, 1983
38) Brewster, N. R., P. S. Freier, and C. J. Waddington, *Astrophys. J.* **294**, 419, 1985
39) Israel, M. H. *12th Texas Symposium on Relativistic Astrophysics*, ed M. Livio & G. Shaviv, in *Ann. NY Acad Sci* **470**, 188, 1984
40) Meyer, J. P., *Proc. 19th Int. Cosmic Ray Conf. (La Jolla)* **9**, 141, 1985
41) Letaw, J. R., R. Silberberg, and C. H. Tsao, *Astrophys. J.* **279**, 144, 1980
42) Binns, W. R., R. K. Fickle, T. L. Garrard, M. H. Israel, J. Klarmann, E. C. Stone, and C. J. Waddington, *Astrophys. J.* **247**, L115, 1981
43) Binns, W. R., D. P. Grossman, M. H. Israel, Michael D. Jones, J. Klarmann, T. L. Garrard, E. C. Stone, R. K. Fickle, and C. J. Waddington, *Proc. 18th Int. Cosmic Ray Conf. (Bangalore)* **9**, 106, 1983
44) Newport, B.J., "The Abundances of Ultraheavy Elements in the Cosmic Radiation", Ph.D. Thesis, California Institute of Technology, 1986
45) Ormes, J. F. and R. J. Protheroe, *Astrophys. J.* **272**, 756, 1983
46) Brewster, N. R., "The Propagation of Ultraheavy Cosmic Rays", Ph.D Thesis, University of Minnesota, 1984
47) Silberberg, R. and C. H. Tsao, *Astrophys. J. Supp.* **25**, 315, 1973
48) Silberberg, R. and C. H. Tsao, *Astrophys. J. Supp.* **25**, 335, 1973
49) Tsao, C. H. and R. Silberberg, *Proc. 16th Int. Cosmic Ray Conf. (Kyoto)* **2**, 202, 1979
50) Silberberg, R., C. H. Tsao, and J. R. Letaw, *Astrophys. J. Supp.* **58**, 873, 1985
51) Waddington, C. J., W. R. Binns, J. R. Cummings, T. L. Garrard, P. S. Gibner, M. H. Israel, M. P. Kertzman and J. Klarmann, *Proc. 20th Int. Cosmic Ray Conf. (Moscow)* **2**, 149, 1987
52) Waddington, C. J., W. R. Binns, T. L. Garrard, M. H. Israel, M. P. Kertzman, J. Klarmann, and E. C. Stone, *Proc. 20th Int. Cosmic Ray Conf. (Moscow)* **2**, 152, 1987
53) Fowler, P. H., M. R. W. Masheder, R. T. Moses, and A. Worley, *Proc. 16th Int. Cosmic Ray Conf. (Kyoto)* **12**, 338, 1979
54) Binns W. R., M. H. Israel, J. Klarmann, W. R. Scarlett, E. C. Stone, and C. J. Waddington, *Nucl. Instr. Meth.* **185**, 415, 1981
55) Fowler, P. H., R. N. F. Walker, M. R. W. Masheder, R. T. Moses, A. Worley,

and A. M. Gay, *Astrophys. J.* **314**, 739, 1987

56) Binns, W. R., R. K. Fickle, T. L. Garrard, M. H. Israel, J. Klarmann, K. E. Krombel, E. C. Stone, and C. J. Waddington, *Astrophys. J.* **267**, L93, 1983

57) Binns, W. R., R. K. Fickle, T. L. Garrard, M. H. Israel, J. Klarmann, E. C. Stone, and C. J. Waddington, *Astrophys. J.* **261**, L117, 1982

58) Cameron, A. G. W., "Elementary and Nuclidic Abundances in the Solar System", *Essays in Nuclear Astrophysics, Proceedings of the Fowler Conference*, edited by C. A. Barnes, D. D. Clayton, and D. N. Schramm, Cambridge University Press, 23, 1982

59) Binns, W. R., T. L. Garrard, P. S. Gibner, M. H. Israel, M. P. Kertzman, J. Klarmann, B. J. Newport, E. C. Stone, and C. J. Waddington, *Astrophys. J.* in preparation, 1989

60) Stone, E. C., C. J. Waddington, W. R. Binns, T. L. Garrard, P. S. Gibner, M. H. Israel, M. P. Kertzman, J. Klarmann, and B. J. Newport, *Proc. 20th Int. Cosmic Ray Conf. (Moscow)* **1**, 366, 1987

61) Stone, E. C., T. L. Garrard, K. E. Krombel, W. R. Binns, M. H. Israel, J. Klarmann, N. R. Brewster, R. K. Fickle, and C. J. Waddington *Proc. 18th Int. Cosmic Ray Conf. (Bangalore)* **9**, 115, 1983

62) Blake, J. B., and S. H. Margolis, *Astrophys. J.* **251**, 402, 1981

63) Binns, W. R., T. L. Garrard, M. H. Israel, Michael D. Jones, M. P. Kamionkowski, J. Klarmann, E. C. Stone, and C. J. Waddington, *Astrophys. J.* **324**, 1106, 1988

64) Grevesse, N. and J. P. Meyer, *Proc. 19th Int. Cosmic Ray Conf. (La Jolla)* **3**, 5, 1985

65) Schramm, D. N., "The R-process and Nucleocosmochronology", *Essays in Nuclear Astrophysics, Proceedings of the Fowler Conference*, edited by C. A. Barnes, D. D. Clayton, and D. N. Schramm, Cambridge University Press, 325, 1982

66) Klarmann, J., W. R. Binns, M. H. Israel, S. H. Margolis, T. L. Garrard, E. C. Stone, N. R. Brewster, D. J. Fixsen, and C. J. Waddington, *Proc. 18th Int. Cosmic Ray Conf. (Bangalore)* **2**, 220, 1983

67) Margolis, S. H., *Proc. 18th Int. Cosmic Ray Conf. (Bangalore)* **9**, 267, 1983

68) Silberberg, R., C. H. Tsao, J. R. Letaw, M. M. Shapiro, *Phys. Rev. Lett.* **51**, 1217, 1983.

69) Margolis, S. H., and J. B. Blake, *Astrophys. J.* **299**, 334, 1985